A class of dynamic mixed models for explicitly filtered LES

By S. T. Bose AND P. Moin

1. Introduction

High Reynolds number wall bounded flows appear in a variety of engineering applications ranging from external aerodynamics to atmospheric boundary layers. The resolution requirements necessary to perform direct numerical simulation of high Reynolds number flows renders DNS infeasible. Use of a subgrid/subfilter closure model makes LES an attractive option, but constructing accurate closure models for the near wall region has proved difficult. In most evaluations of the performance of subgrid/subfilter closure models in wall bounded flows, the LES resolution is chosen to be relatively fine, roughly a factor of three to four coarser than the resolution required for DNS along wall parallel directions. Figure 1 shows the streamwise and spanwise resolutions for a small survey of studies that were primarily interested in the development of new or improved closure models. These models were primarily tested in channel flow simulations, although the validation test case used in the rescaling procedure of Lund *et al.* (1998) in a boundary layer is also included. Results from LES of wall bounded flows using a variety of closure models are often satisfactory when a $\Delta x^+ \approx 50$ and $\Delta z^+ \approx 20 - 30$ are used. Undoubtedly, simulations of very high Reynolds number wall bounded flows will require use of an explicit wall model coupled to an outer LES. However, further development of subfilter closure models for LES may allow simulations of higher Reynolds numbers for wall-resolved LES and may facilitate more accurate simulations for the validation of wall-modeled LES.

The model development pursued here will use the governing equations for explicitly filtered LES. Because the performance of the model is of primary interest, the use of a framework that is able to isolate subfilter closure model errors from numerical errors is necessary. Previous simulations have shown that the model errors can be isolated by maintaining a fixed filter width and performing grid refinement studies (Bose *et al.* 2010). The governing equations for explicit filtered LES for incompressible flows are

$$\bar{u}_i = \int_\Omega G(x, x') u_i(x') dx' \tag{1.1}$$

$$\frac{\partial \bar{u}_i}{\partial t} + \frac{\partial \overline{\bar{u}_i \bar{u}_j}}{\partial x_j} = -\frac{\partial \bar{p}}{\partial x_j} + \frac{1}{Re} \frac{\partial^2 \bar{u}_i}{\partial x_j \partial x_j} - \frac{\partial \tau_{ij}}{\partial x_j} \tag{1.2}$$

$$\tau_{ij} = \overline{u_i u_j} - \overline{\bar{u}_i \bar{u}_j}, \tag{1.3}$$

with the remaining condition that the filtered velocity field, $\bar{u}_i$, is solenoidal. The objective of the present investigation is to evaluate the performance of subfilter closure models at relatively coarse resolutions for LES. A class of mixed models for the subfilter stress tensor in the explicitly filtered LES framework is presented in Section 2. Discussion of the eddy viscosity models and an analysis of the $k|\bar{S}|^{-1}$ eddy viscosity is presented in Section 3. The numerical method and the models considered are outlined in Section 4,

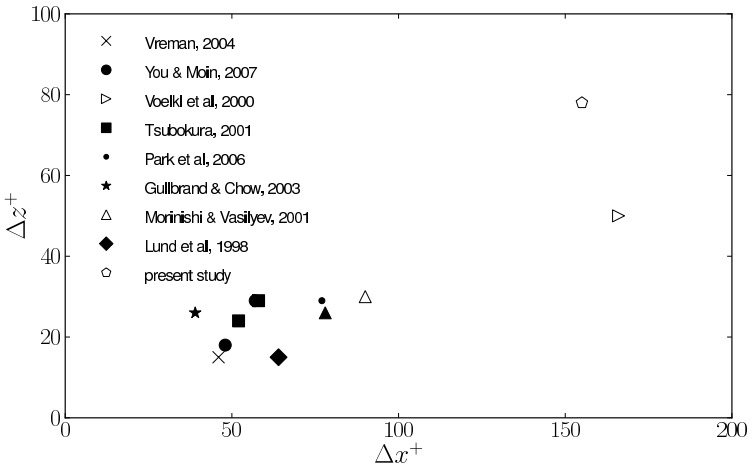

FIGURE 1. Streamwise (Δx^+) and spanwise (Δz^+) resolutions for small survey of wall bounded LES calculations where the performance of the subfilter/subgrid scale model was investigated. Open symbols denote simulations for $Re_\tau > 1000$ and closed symbols denote simulations for $Re_\tau < 1000$.

and an assessment of these models in an $Re_\tau = 2000$ channel flow is presented in Section 5. Concluding remarks are made in Section 6.

2. Subfilter scale modeling for explicitly filtered LES

2.1. *Model formulation*

In the implicitly filtered LES formulation, the deviatoric component of the subgrid stress tensor is often approximated with an eddy viscosity closure (Germano *et al.* 1991; Vreman 2004):

$$\tau_{ij}^{*,imp} = (\overline{u_i u_j} - \bar{u}_i \bar{u}_j)^* \approx -2\nu_t \bar{S}_{ij}. \tag{2.1}$$

Other models of τ_{ij}^{imp} assume a scale similarity of the velocity field between u and $\bar{u}$ (Bardina *et al.* 1980; Zang *et al.* 1993):

$$\tau_{ij}^{imp} = \overline{u_i u_j} - \bar{u}_i \bar{u}_j \approx \overline{\bar{u}_i \bar{u}_j} - \bar{\bar{u}}_i \bar{\bar{u}}_j. \tag{2.2}$$

Here, we attempt a systematic approach to modeling the subfilter stress tensor that arises in explicit filtering:

$$\tau_{ij} = \overline{u_i u_j} - \overline{\bar{u}_i \bar{u}_j} = C_{ij} + R_{ij} \tag{2.3}$$

$$u_i' = u_i - \bar{u}_i \tag{2.4}$$

$$C_{ij} = \overline{u_i' \bar{u}_j} + \overline{\bar{u}_i u_j'} \tag{2.5}$$

$$R_{ij} = \overline{u_i' u_j'}, \tag{2.6}$$

where C_{ij} are the cross stresses and R_{ij} is the Reynolds stress. The Leonard stress that

appears in the expansion of τ_{ij}^{imp} is incorporated into the convective term in Eq. 1.2. The assumption that the subgrid scales are purely dissipative (as is implied by Eq. 2.1) has been justified *a posteriori* in a number of calculations. The success of the eddy viscosity model has then suggested that it is possible to accurately model the subgrid stress tensor by primarily capturing the dissipation that the SGS tensor provides without necessarily capturing its energetics or structure. In many of these simulations, the energetics of the subgrid scales are insignificant compared to the energy contained in the resolved scales, as evidenced by the comparison of the *unfiltered* root mean square (rms) fluctuations with the *resolved* rms fluctuations. However, the energetics of the subgrid (subfilter) stress tensor may be significant when the LES is coarse and much of the turbulence remains unresolved. This particular situation often arises in high Reynolds number flows where computational expense prohibits the use of finer resolution. The approach in the following is to model each of the component stresses (C_{ij}, R_{ij}) in Eq. 2.3 directly. Note that the Leonard stress in the explicitly filtered LES equations is subsumed into the convective term and therefore, does not appear in Eq. 2.3.

Consider the first half of the cross stresses, $\overline{u_i'\bar{u}_j}$ (the following analysis can be repeated again for $\overline{\bar{u}_i u_j'}$), which is defined as

$$\overline{u_i'\bar{u}_j}(x) = \int_\Omega G(x,x')u_i'(x')\bar{u}_j(x')dx'. \tag{2.7}$$

We will now assume that the resolved velocity field, $\bar{u}_j$, is smooth over the space spanned by the filter width. It is known that this assumption is always violated; for any given filter width (Δ_f) that is larger than the Kolmogorov scale, there will be an eddy whose characteristic length scale is Δ_f. However, the assumption is potentially admitted because the energy contained at scales larger than Δ_f is significantly larger than that from the eddies at Δ_f. Using this assumption, Eq. 2.7 can be approximated as

$$\int_\Omega G(x',x)u_i'(x')\bar{u}_j(x')dx' \approx \bar{u}_j(x)\int_\Omega G(x',x)u_i'(x')dx' = \overline{u'}_i(x)\bar{u}_j(x). \tag{2.8}$$

By filtering Eq. 2.4, an exact expression for $\overline{u'}_i$ can be derived:

$$\overline{u'}_i = \bar{u}_i - \bar{\bar{u}}_i, \tag{2.9}$$

thus, closing the expression on the right-hand side of Eq. 2.8. Then, the cross stresses are modeled as

$$C_{ij} \approx \bar{u}_i\overline{u'}_j + \overline{u'}_i\bar{u}_j. \tag{2.10}$$

We now will perform a similar expansion for the Reynolds stress, R_{ij} although the assumption of a smooth resolved velocity field in Eq. 2.8 is now violated.

$$\begin{aligned} R_{ij} = \overline{u_i'u_j'} &= \int_\Omega G(x',x')u_i'(x')u_j'(x')dx' \\ &= \int_\Omega G(x',x')u_i'(x')\left(\overline{u'}_j(x) + O(\Delta_f^s)\right)dx' \qquad (2.11) \\ R_{ij} &\approx \overline{u'}_i\overline{u'}_j - 2\nu_t\bar{S}_{ij}, \qquad (2.12) \end{aligned}$$

where s the measure of accuracy of this expansion. However, because it is impossible to bound higher order derivatives of the unfiltered velocity field (see the discussion in Vreman *et al.* 1996), the value of s is resolution and flow dependent. Because the first term in the approximation of the Reynolds stress will not adequately express the small-scale dissipation, we have added an eddy viscosity term to Eq. 2.12. Collecting Eq. 2.10 and Eq. 2.12 yields the full subfilter closure model

$$\tau_{ij} \approx \bar{u}_i \overline{u'}_j + \overline{u'}_i \bar{u}_j + \overline{u'}_i \overline{u'}_j - 2\nu_t \bar{S}_{ij} \tag{2.13}$$

$$= \eta_{ij} - 2\nu_t \bar{S}_{ij}. \tag{2.14}$$

Specification of the eddy viscosity, ν_t, will be made in a later section, and the simulations considered in this study will consider the effect of using different eddy viscosity models.

2.2. *Galilean invariance*

Speziale (1985) showed that the explicitly filtered LES equations in Eq. 1.2 are not necessarily Galilean invariant. It was shown that although the standard eddy viscosity models are themselves Galilean invariant, the resultant explicitly filtered LES equation is not. We will now show that the use of the subfilter closure model in Eq. 2.13 makes the explicitly filtered LES equations Galilean invariant provided the added eddy viscosity model is also Galilean invariant.

We briefly outline the proof of Galilean invariance below, but some of the details follow exactly the derivation of Speziale and can be found in his work. Let us consider a Galilean transformation of the velocity field by a fixed velocity vector, V,

$$x_i^* = x_i + V_i t + b_i, \tag{2.15}$$

$$u_i^* = u_i + V_i. \tag{2.16}$$

Given the frame invariance of a function, $\phi^* = \phi$, it then follows that

$$\bar{\phi}^* = \int_\Omega G^*(x'^* - x^*, \Delta_f^*)\phi^*(x'^*)dx'^*$$

$$= \int_\Omega G(x' - x, \Delta_f)\phi(x')dx' = \bar{\phi} \tag{2.17}$$

by some simple manipulation of Eq. 2.15 (see Eqns. 24-26 in Speziale 1985). The above expression holds even for nonuniform filter widths. The filter kernel G is only a function of $x' - x$, although the filter width is allowed to vary; for a Gaussian filter kernel, this is equivalent to saying that kernel is always centered at x while the standard deviation (σ) of the filter kernel is allowed to vary in space. From differentiation of Eq. 2.15,

$$\frac{\partial}{\partial x_j^*} = \frac{\partial}{\partial x_j}, \tag{2.18}$$

$$\frac{\partial}{\partial t^*} = \frac{\partial}{\partial t} - V_j \frac{\partial}{\partial x_j}. \tag{2.19}$$

Then, the addition of the convective term and subfilter stress model excluding the eddy viscosity term, η_{ij} (Eq. 2.14),

$$\left(\overline{\bar{u}^*{}_i \bar{u}^*{}_j} + \eta^*_{ij}\right),_j = (\overline{\bar{u}_i \bar{u}_j} + V_i \bar{\bar{u}}_j + \bar{\bar{u}}_i V_j + V_i V_j + 3\,(\bar{u}_i + V_i)\,(\bar{u}_j + V_j)$$
$$+ (\bar{\bar{u}}_i + V_i)\,(\bar{\bar{u}}_j + V_j) - 2\,(\bar{\bar{u}}_i + V_i)\,(\bar{u}_j + V_j) - 2\,(\bar{u}_i + V_i)\,(\bar{\bar{u}}_j + V_j)),_j \tag{2.20}$$
$$= (\overline{\bar{u}_i \bar{u}_j} + \eta_{ij})\,,_j + V_j \bar{u}_{i,j}. \tag{2.21}$$

Combining the above result with the expression for the time derivative, we observe that

$$\frac{\partial \bar{u}^*_i}{\partial t} + \left(\overline{\bar{u}^*_i \bar{u}^*_j} + \eta^*_{ij}\right),_j = \frac{\partial \bar{u}_i}{\partial t} + (\overline{\bar{u}_i \bar{u}_j} + \eta_{ij})\,,_j\,. \tag{2.22}$$

Therefore, the full explicitly filtered LES equation is Galilean invariant. We refer the reader to Speziale for the proof that the remaining terms, including the eddy viscosity closure, are also Galilean invariant.

2.3. *Relationship of η_{ij} to approximate deconvolution methods*

The approximate deconvolution method of Stolz *et al.* (2001) attempts to deconvolve the filtered velocity using a van Cittert iteration

$$u^N_i = \sum_{k=0}^{N} (I - G)^k \star \bar{u}_i. \tag{2.23}$$

The LES equations solved are

$$\frac{\partial \bar{u}_i}{\partial t} + \frac{\partial}{\partial x_j}\left(\overline{u^N_i u^N_j}\right) = -\frac{\partial p}{\partial x_i} + \frac{1}{Re}\frac{\partial^2 \bar{u}_i}{\partial x_j \partial x_j} - \chi, \tag{2.24}$$

where χ is a purely dissipative term. If we consider a linear deconvolution model, $N = 1$ in Eq. 2.23, then

$$u^1_i = \bar{u}_i + \bar{u}_i - \bar{\bar{u}}_i = \bar{u}_i + \overline{u'}_i \tag{2.25}$$
$$\overline{u^1_i u^1_j} = \overline{\bar{u}_i \bar{u}_j} + \overline{\eta}_{ij}. \tag{2.26}$$

If the model terms proposed in η_{ij} are filtered, then the sum of the convective term and $\overline{\eta}_{ij}$ is equivalent to a linear deconvolution model. However, filtering η_{ij} would invalidate the Galilean invariance that was constructed above.

3. Eddy viscosity models

3.1. *Representations of the eddy viscosity*

In the formulation of Eq. 2.13, the choice of the form of the eddy viscosity has yet to be specified. We consider the performance of three different choices of the eddy viscosity: a Smagorinsky eddy viscosity, a Vreman eddy viscosity, and a $k|\bar{S}|^{-1}$ eddy viscosity.

$$\nu_t = C\Delta^2 |\bar{S}|, \tag{3.1}$$
$$\nu_t = C\sqrt{\frac{B_\beta}{\bar{\alpha}_{ij}\bar{\alpha}_{ij}}}, \tag{3.2}$$
$$\nu_t = C k_{sgs} |\bar{S}|^{-1}. \tag{3.3}$$

where $\alpha_{ij} = \frac{\partial u_j}{\partial x_i}$ and B_β is an invariant of $\alpha^T\alpha$. The eddy viscosity kernel in Eq. 3.3 has not been frequently used in the literature; it has been proposed in the past by Tsubokura (2001) and Sagaut (1996). In the latter, the $k_{sgs}|\bar{S}|^{-1}$ model is the limit of the mixed scale model ($\nu_t = C|\bar{S}|^\alpha k^{(1-\alpha)/2}\Delta^{1+\alpha}$) with the choice of the parameter $\alpha = -1$. Tsubokura investigated the use of this model in LES of low Reynolds number channel flows and obtained good agreement with DNS for the mean velocity profile and rms statistics. The proposition by Tsubokura was that this model was better suited for the dynamic procedure because it did not require a specification of a length scale ratio ($\frac{\Delta_T}{\Delta_g}$) and better correlated numerically with the Leonard stress. It was based on these tenets that Tsubokura explained the observed agreement with the DNS data.

3.2. *Sensitivity to the choice of k_{sgs} in the $k|\bar{S}|^{-1}$ model*

The model in Eq. 3.3 requires the specification of how the subgrid kinetic energy, k_{sgs}, is estimated. Ghosal *et al.* (1995) and Kim & Menon (1995) have suggested the transport of an equation for k_{sgs} where the coefficients in the transport equation are derived through the extension of Germano *et al.*'s dynamic procedure. Care should be taken in extending this approach to the current work as the particular forms of $k_{sgs} = \frac{1}{2}\tau_{ii}$ differ due to the inclusion of the Leonard stress into the convective term in the explicitly filtered formulation. This method is not considered in the current work.

In order to simplify the model and reduce computational expense, we will estimate k_{sgs} purely from the resolved quantities. There are several estimates that are investigated at present:

$$k_{sgs} = \frac{1}{2}\sum_{i,k}\Delta_k^2\frac{\partial\bar{u}_i}{\partial x_k}\frac{\partial\bar{u}_i}{\partial x_k} \tag{3.4}$$

$$k_{sgs} = \frac{1}{2}\overline{u'}_i\overline{u'}_i \tag{3.5}$$

$$k_{sgs} = -\frac{1}{2}\left(\overline{\bar{u}_i\bar{u}_i} - \bar{u}_i\bar{u}_i\right). \tag{3.6}$$

Eq. 3.4 derives its estimate from the trace of the gradient model (Clark *et al.* 1979), Eq. 3.5 is related to the kinetic energy of the unresolved velocity field projected onto the filter space, and Eq. 3.6 is the negative of the trace of the Leonard stress. Note that if we chose $k_{sgs} = C\Delta^2|\bar{S}|^2$ as suggested by Yoshizawa (1986), then we would once again arrive at the Smagorinsky model. The eddy viscosity in Eq. 3.3 is not necessarily Galilean invariant for all choices of k_{sgs}. In this investigation, the specifications of k_{sgs} using Eq. 3.4 and Eq. 3.5 are Galilean invariant, while Eq. 3.6 is not.

3.3. *Relationship of $k|\bar{S}|^{-1}$ to existing SGS models*

The eddy viscosity representation in Eq. 3.3 is closely related to the stretched vortex model of Misra & Pullin (1997). The stretched vortex model represents the subfilter stress as

$$\tau_{ij} = k_{sgs}\left(\delta_{ij} - e_i^v e_j^v\right), \tag{3.7}$$

where e^v is the unit vector denoting the alignment of the assumed strained vortex. One simple model for e^v that has successfully been used in shear flows and in isotropic turbulence (Voelkl *et al.* 2000; Pantano *et al.* 2008; Misra & Pullin 1997) is to assume that e^v

is aligned with the eigenvector of $\bar{S}_{ij}$ with the largest extensional strain ($\lambda_3 = \max_i \lambda_i$). Under this assumption, the subgrid dissipation can be expressed as

$$\epsilon_{sgs} = -\tau_{ij}\bar{S}_{ij} = k_{sgs}\lambda_3 = k_{sgs}|\bar{S}|\cos(\phi) \tag{3.8}$$

$$\phi = \frac{1}{3}\tan^{-1}\frac{\sqrt{p^3 - q^2}}{q},\ p = \frac{1}{6}\sum_{i,j}\bar{S}_{ij}^2,\ q = \frac{1}{2}\det(\bar{S}). \tag{3.9}$$

The subgrid dissipation of the model in Eq. 3.3 is given as

$$\epsilon_{sgs} = -\tau_{ij}\bar{S}_{ij} = Ck_{sgs}|\bar{S}|. \tag{3.10}$$

Both the stretched vortex model and the $k|\bar{S}|^{-1}$ model will scale the subfilter dissipation with $|\bar{S}|$, although the exact amount of the dissipation in space may still be quite different due to differences between C and $\cos(\phi)$.

4. Numerical method and cases considered

We consider a fixed pressure gradient driven $Re_\tau = 2000$ channel flow as the test case by which to evaluate the different SGS models. A fourth-order finite difference code based on the numerics of Morinishi *et al.* (1998) and the discrete, commuting filters of Vasilyev *et al.* (1998) are used to solve the explicitly filtered LES equations. For all simulations, the filter width is set at $\Delta x^+ \approx 155$, $\Delta z^+ \approx 78$, and $\Delta y_f^+ \approx 95$, corresponding to the filter widths in the streamwise direction, spanwise direction, and the wall-normal direction measured at the centerline. The filter width in the wall-normal direction is reduced as the wall is approached, and Δy_f^+ is less than 1 at the wall. At this resolution, the dominant near-wall structures are wholly unrepresented by the resolved motions requiring an accurate closure model to correctly represent the dynamics of the large-scale motions. A more detailed description of the numerical method and the generation of the initial condition can be found in Bose *et al.* (2010). However, the statistical window used here is not equivalent to the previous study. At the present time, the calculations have been limited to $H/u_\tau \approx 15$ with the statistical sampling window performed over the last 5 time units, where H is the half-height of the channel. The mean velocity profiles are statistically converged during this time window when compared to samples from sampling windows of $H/u_\tau = 8 - 10$ and $H/u_\tau = 15 - 17$ (for the 2 cases that were integrated further in time). The statistical sampling errors are most apparent in the errors reported in the mean centerline velocity and in the rms velocity profiles, particularly near the centerline of the channel.

The following subfilter closure models are evaluated: dynamic Smagorinsky, dynamic mixed Smagorinsky, dynamic mixed $k|\bar{S}|^{-1}$ model, and a dynamic mixed Vreman model. The class of these three dynamic mixed models differ only in their specification of the eddy viscosity in Eq. 2.13. Unless otherwise specified, we will utilize Eq. 3.5 as the surrogate for k_{sgs} in the mixed $k|\bar{S}|^{-1}$ model. The coefficient in the eddy viscosity for the Smagorinsky models is allowed to vary as a function of wall-normal distance, $C(y)$, whereas the eddy viscosity coefficient for the $k|\bar{S}|^{-1}$ and Vreman models are global constants. In the case of the global coefficient, the dynamic procedure follows Lee *et al.* (2010), where the modified Germano identity is averaged over the entire volume to yield the global coefficient. A summary of the LES performed is given in Table 1.

N_x	N_y	N_z	L_x	L_y	L_z	Δx_f^+	Δz_f^+	Δy_f^+ (c)
256	192	256	4π	2	2π	155	78	95

TABLE 1. Summary of the parameters for all simulations of an $Re_\tau = 2000$ channel flow. Lengths are non-dimensionalized by the channel half height, H, and velocities are non-dimensionalized by the friction velocity, u_τ.

5. Results and discussion

Figure 2 shows the mean velocity profile for the dynamic Smagorinsky model, the dynamic mixed $k|\bar{S}|^{-1}$ model, and the filtered DNS of Hoyas & Jiménez (2006). The difference between the filtered mean velocity profile and the unfiltered mean velocity profile from the DNS data is negligible for the chosen filter. The overshoot in the prediction of the mean velocity in the buffer layer has been observed frequently for the dynamic Smagorinsky model when the LES resolution is coarse. It is apparent that the dynamic Smagorinsky model overpredicts the streamwise mean velocity profile throughout the channel. However, the dynamic mixed $k|\bar{S}|^{-1}$ model is able to correctly predict the mean velocity in the near-wall region ($y^+ < 200$). For $y^+ > 200$, the dynamic mixed $k|\bar{S}|^{-1}$ model initially underpredicts the mean velocity but overestimates the velocity as the channel centerline is approached. The error in the mean velocity at the centerline is reduced by half by the mixed $k|\bar{S}|^{-1}$ model when compared to the dynamic Smagorinsky model. Figure 3 shows the mean velocity profiles for the three different mixed models considered. The overshoot in the mean velocity prediction in the buffer layer experienced by the dynamic Smagorinsky model is corrected by all three of the mixed models. Therefore, it is concluded that the addition of the similarity-like terms provides sufficient Reynolds stress (τ_{12}) in the near-wall region to accurately capture the mean. The dynamic mixed Smagorinsky model overpredicts the filtered DNS mean velocity profile through the domain and its slope in the log law region is also overpredicted ($\kappa \approx 0.34$). Both the mixed Vreman and mixed $k|\bar{S}|^{-1}$ models exhibit similar behavior where the mean velocity is underpredicted in the region $200 < y^+ < 1000$, and the mean velocity is overpredicted for $1000 < y^+ < 2000$. The maximum error in the mean velocity profile is roughly 3.5% for both the mixed $k|\bar{S}|^{-1}$ model and the mixed Vreman model observed near $y^+ \approx 400$. Although there are some differences in the mean velocity profiles of these two models, it is difficult to distinguish them in terms of the quality of their mean velocity profile predictions. The bulk velocity, U_b, however, is almost exactly captured by both the mixed $k|\bar{S}|^{-1}$ and mixed Vreman models, whereas it is overestimated by both the dynamic Smagorinsky and mixed Smagorinsky models by about 5%. It is unclear whether the small errors in the prediction of U_b by the mixed $k|\bar{S}|^{-1}$ and mixed Vreman models is merely fortuitous or due to superior model performance. Table 2 lists the predictions and errors in the values of the bulk velocity, U_b, and the channel centerline velocity, U_c.

Because of the relatively poor prediction of the mean velocity profile by the standard dynamic Smagorinsky model, we will restrict further evaluation to the class of dynamic mixed models. Figure 4 shows the prediction of the rms velocity fluctuations compared to filtered DNS. Further from the wall, the streamwise rms fluctuations are nearly identical while small differences can be observed in the predictions of the spanwise ($\bar{w}'$) and wall-

	U_b	U_c	% error U_b	% error U_c
DNS (Hoyas & Jiménez 2006)	21.75	24.29	–	–
Dynamic Smagorinsky	22.73	25.43	4.5	4.7
Dynamic mixed Smagorinsky	22.91	25.89	5.4	6.6
Dynamic mixed Vreman	21.88	24.85	0.6	2.3
Dynamic mixed $k\|\bar{S}\|^{-1}$	21.76	24.88	0.05	2.4

TABLE 2. Errors in the prediction of the bulk velocity, U_b, and centerline velocity, U_c, for the different LES models. Due to potentially insufficient statistical sampling, errors in the centerline velocity fluctuate by about 0.4%.

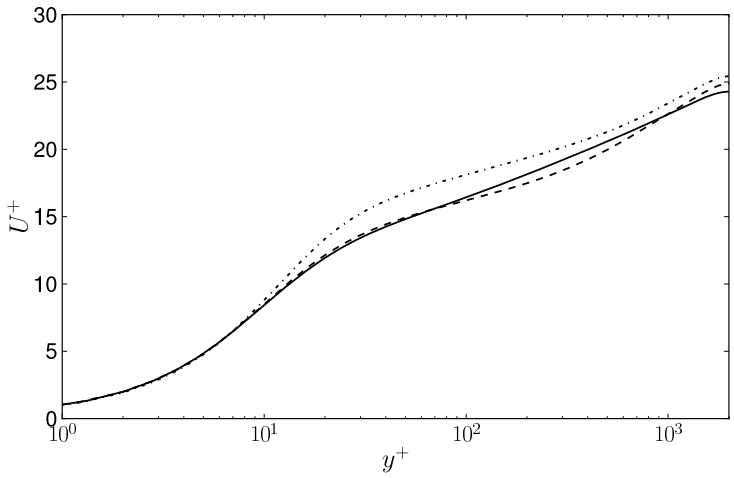

FIGURE 2. Streamwise mean velocity profile for a turbulent channel flow at $Re_\tau = 2000$ using the dynamic Smagorinsky model $(- \cdot -)$ and the dynamic mixed $k|\bar{S}|^{-1}$ model $(- -)$ compared with the filtered DNS of Hoyas & Jiménez (2006) $(-)$.

normal ($\bar{v}'$) fluctuations. The Vreman model shows the best prediction of the $\bar{v}'$ and $\bar{w}'$ fluctuations, but the differences between all three of the models is small when compared against the local mean velocity. Near the wall, the $\bar{w}'$ fluctuation is largely underestimated by the mixed Smagorinsky and mixed Vreman models; the mixed $k|\bar{S}|^{-1}$ model is better at capturing this near-wall behavior, although there is slight overprediction of the peak $\bar{w}'$. For the mixed $k|\bar{S}|^{-1}$ model, this overprediction of the filtered near-wall fluctuations is more pronounced in $\bar{v}'$. All the models substantially underestimate the turbulent fluctuations near the center of the channel. Although comparison of the filtered velocity fluctuations is the most honest assessment of the closure model because the governing equation is solved for filtered quantities, it is often that the physical (unfiltered) fluctuations are of more interest. The unfiltered Reynolds stress tensor can be approximated by

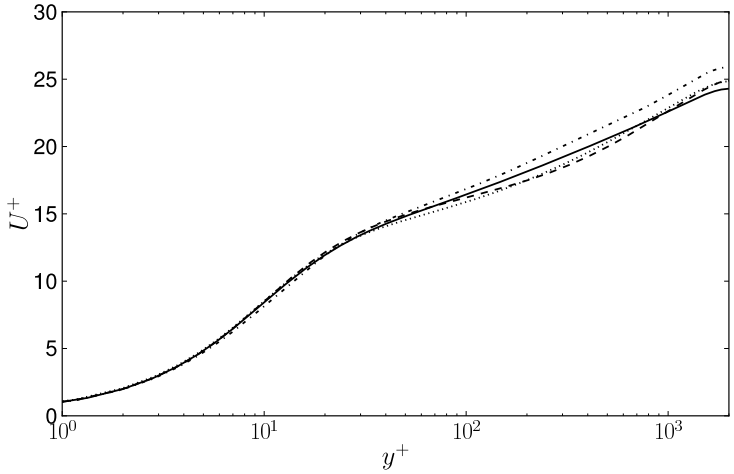

FIGURE 3. Streamwise mean velocity profile for a turbulent channel flow at $Re_\tau = 2000$ using the dynamic mixed Smagorinsky $(- \cdot -)$, dynamic mixed $k|\bar{S}|^{-1}$ $(- -)$, and dynamic mixed Vreman $(\cdots)$ models compared with the filtered DNS of Hoyas & Jiménez (2006) $(-)$.

$$\langle u_i u_j \rangle \approx \langle \overline{\bar{u}_i \bar{u}_j} \rangle + \langle \tau_{ij} \rangle, \tag{5.1}$$

where $\langle \cdot \rangle$ denotes the average along the streamwise and spanwise directions and in time. By commuting the $\langle \cdot \rangle$ averaging operator with the filtering operator in the first term on the right-hand side, it is possible to obtain an approximation of $\langle u_i u_j \rangle$ without storing the entire averaged 3D $\overline{\bar{u}_i \bar{u}_j}$ field for this case. In order to estimate the physical rms fluctuations, we further assume that $\langle u \rangle = \langle \bar{u} \rangle$, which is valid for this case. Figure 5 compares the physical rms fluctuations obtained from the mixed Vreman model, mixed $k|\bar{S}|^{-1}$ model, and the DNS of Hoyas & Jiménez (2006). Away from the wall, predictions of the rms fluctuations from the two models are similar. However, for $y^+ < 100$, the mixed $k|\bar{S}|^{-1}$ model better captures the near-wall peaks, especially in the w' and v' fluctuations. Although the mixed $k|\bar{S}|^{-1}$ model had overpredicted the filtered $\bar{v}'$ and $\bar{w}'$ fluctuations, it still slightly underpredicts the peak values of the physical rms fluctuations. Both models again underestimate the fluctuations at the channel centerline. Figure 6 shows the Reynolds shear stress contributions from the resolved scales, the subfilter model, and their sum for the dynamic mixed $k|\bar{S}|^{-1}$ model. Because the LES resolution is so coarse, the subfilter stress model provides a large fraction of the total stress. At some locations in the near-wall region, the subfilter model stress exceeds the contribution from the resolved scales, confirming the assertion that the resolution chosen exposes the importance of the subfilter scale model.

Finally, the sensitivity of the $k|\bar{S}|^{-1}$ model to the choice of the k_{sgs} surrogate is investigated. Figure 7 shows the mean velocity profile obtained from using three different choices of the k_{sgs} surrogate shown in Eqs. 3.4 - 3.6. The mean velocity profiles here show little sensitivity to the particular choice of k_{sgs}. Eq. 3.5 was chosen in the previous analysis because it produced the best results when estimating the physical (unfiltered) rms velocity fluctuations.

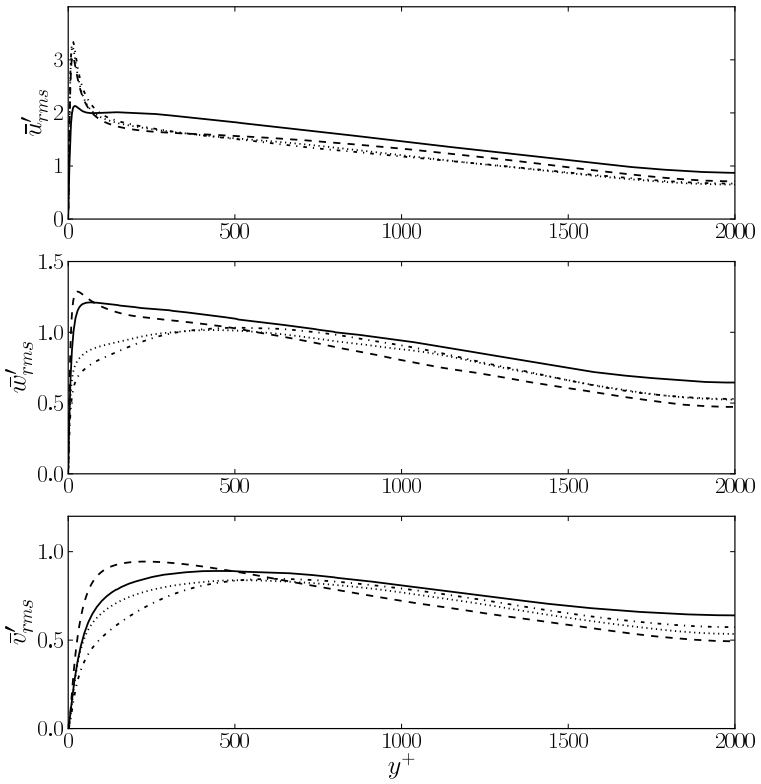

FIGURE 4. Rms velocity profiles for the filtered velocity field for the dynamic mixed Smagorinsky $(-\cdot-)$, dynamic mixed $k|\bar{S}|^{-1}$ $(--)$, and dynamic mixed Vreman $(\cdots)$ compared to the filtered DNS of Hoyas & Jiménez (2006) $(-)$.

6. Concluding remarks

A class of mixed models for the subfilter stress tensor that arises in explicitly filtered LES has been presented. These mixed models were tested using three different representations of the eddy viscosity model and results were compared in coarse calculations of an $Re_\tau = 2000$ channel flow. Relatively accurate predictions of the mean velocity (within $\approx 3.5\%$) were obtained using the dynamic mixed $k|\bar{S}|^{-1}$ model. The dynamic mixed $k|\bar{S}|^{-1}$ model also produced reasonably accurate predictions of the physical (unfiltered) rms fluctuations given the coarse resolution of the LES; in particular, the near-wall peaks in v' and w' are well represented, but the fluctuations at the centerline were underestimated. No additional empiricism or explicit wall model is used in the proposed class of mixed models despite the coarse resolution of the LES. Therefore, it is possible that this class of mixed models will provide better description of the subfilter stress tensor in other flow configurations including those with separation. Grid convergence studies of these models (similar to those by Bose *et al.* 2010) to isolate the model errors from the numerical errors are currently under way. Once grid-independence has been demonstrated, final conclusions on the performance of the closure model will be drawn. Additionally, the

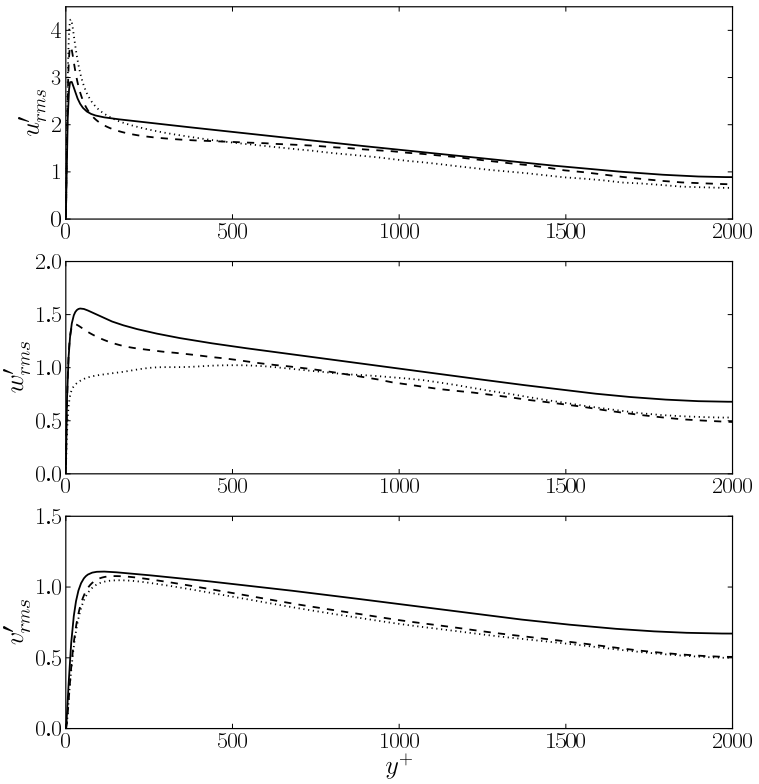

FIGURE 5. Estimation of unfiltered rms velocity fluctuations for the dynamic mixed $k|\bar{S}|^{-1}$ $(- \cdot -)$ and dynamic mixed Vreman $(\cdots)$ compared to DNS (Hoyas & Jiménez 2006) $(-)$.

performance of these mixed models will be tested in other flow configurations in future investigations.

REFERENCES

BARDINA, J., FERZIGER, J. H. & REYNOLDS, W. C. 1980 Improved subgrid scale models for large eddy simulation. *AIAA Paper* **80-1357**.

BOSE, S. T., MOIN, P. & YOU, D. 2010 Grid-independent large-eddy simulation using explicit filtering. *Physics of Fluids* **22** (10), 105103.

CLARK, R. A., FERZIGER, J. H. & REYNOLDS, W. C. 1979 Evaluation of subgrid-scale models using an accurately simulated turbulent flow. *Journal of Fluid Mechanics* **91**, 1–16.

GERMANO, M., PIOMELLI, U., MOIN, P. & CABOT, W. H. 1991 A dynamic subgrid-scale eddy viscosity model. *Physics of Fluids A: Fluid Dynamics* **3** (7), 1760–1765.

GHOSAL, S., LUND, T. S., MOIN, P. & AKSELVOLL, K. 1995 A dynamic localization

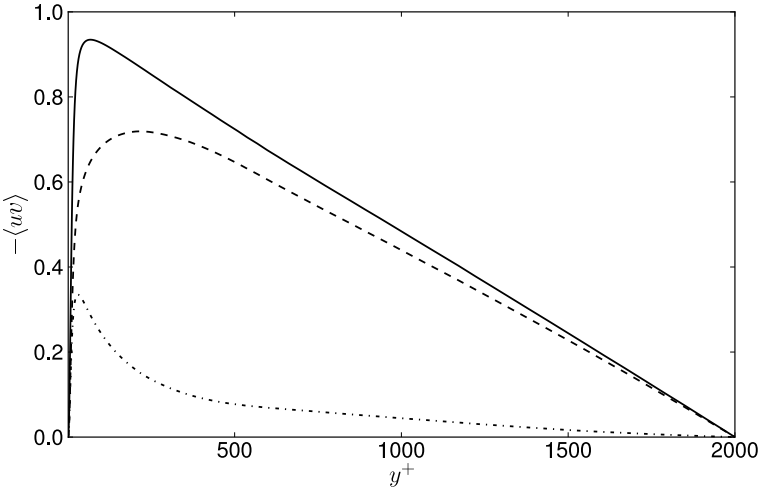

FIGURE 6. Reynolds shear stress contributions from the resolved scales $(- -)$, the subfilter stress model $(- \cdot -)$, and their total sum $(-)$ for the dynamic mixed $k|\bar{S}|^{-1}$ model.

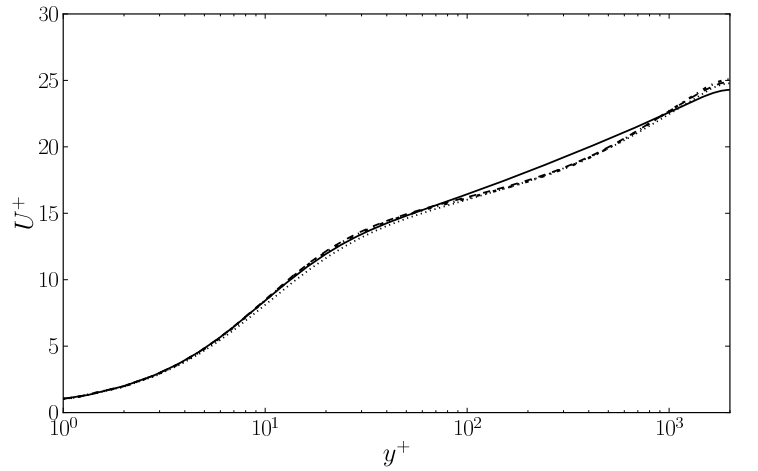

FIGURE 7. Streamwise mean velocity profile for the dynamic mixed $k|\bar{S}|^{-1}$ model using the k surrogate defined in Eq. 3.4 $(\cdots)$, Eq. 3.5 $(- -)$, and Eq. 3.6 $(- \cdot -)$ compared with the filtered DNS of Hoyas & Jiménez (2006).

model for large-eddy simulation of turbulent flows. *Journal of Fluid Mechanics* **297**, 402–402.

HOYAS, S. & JIMÉNEZ, J. 2006 Scaling of the velocity fluctuations in turbulent channels up to $Re_\tau = 2003$. *Physics of Fluids* **18** (1), 011702.

KIM, W. & MENON, S. 1995 A new dynamic one equation subgrid scale model for large eddy simulations. *AIAA Paper* **95-0356**.

Lee, J., Choi, H. & Park, N. 2010 Dynamic global model for large eddy simulation of transient flow. *Physics of Fluids* **22** (7), 075106.

Lund, T., Wu, X. & Squires, K. 1998 Generation of turbulent inflow data for spatially-developing boundary layer simulations. *Journal of Computational Physics* **140**, 233–258.

Misra, A. & Pullin, D. I. 1997 A vortex-based subgrid stress model for large-eddy simulation. *Physics of Fluids* **9** (8), 2443–2454.

Morinishi, Y., Lund, T. S., Vasilyev, O. V. & Moin, P. 1998 Fully conservative higher order finite difference schemes for incompressible flow. *Journal of Computational Physics* **143** (1), 90 – 124.

Pantano, C., Pullin, D. I., Dimotakis, P. E. & Matheou, G. 2008 LES approach for high reynolds number wall-bounded flows with application to turbulent channel flow. *Journal of Computational Physics* **227**, 9271–9291.

Sagaut, P. 1996 Simulations of separated flows with subgrid models. *La Recherche Aerospatiale* **1**, 51–63.

Speziale, C. G. 1985 Galilean invariance of subgrid-scale stress models in the large-eddy simulation of turbulence. *Journal of Fluid Mechanics* **156**, 55–62.

Stolz, S., Adams, N. A. & Kleiser, L. 2001 An approximate deconvolution model for large-eddy simulation with application to incompressible wall-bounded flows. *Physics of Fluids* **13** (4), 997–1015.

Tsubokura, M. 2001 Proper representation of the subgrid-scale eddy viscosity for the dynamic procedure in large eddy simulation using finite difference method. *Physics of Fluids* **13** (2), 500–504.

Vasilyev, O. V., Lund, T. S. & Moin, P. 1998 A general class of commutative filters for LES in complex geometries. *Journal of Computational Physics* **146** (1), 82 – 104.

Voelkl, T., Pullin, D. I. & Chan, D. C. 2000 A physical-space version of the stretched-vortex subgrid-stress model for large-eddy simulation. *Physics of Fluids* **12** (7), 1810–1825.

Vreman, A. 2004 An eddy-viscosity subgrid-scale model for turbulent shear flow: Algebraic theory and applications. *Physics of Fluids* **16** (10), 3670–3681.

Vreman, B., Geurts, B. & Kuerten, H. 1996 Large-eddy simulation of the temporal mixing layer using the Clark model. *Theoretical and Computational Fluid Dynamics* **8**, 309–324.

Yoshizawa, A. 1986 Statistical theory for compressible turbulent shear flows, with the application to subgrid modeling. *Physics of Fluids* **29** (7), 2152–2164.

Zang, Y., Street, R. L. & Koseff, J. R. 1993 A dynamic mixed subgrid-scale model and its application to turbulent recirculating flows. *Physics of Fluids A: Fluid Dynamics* **5** (12), 3186–3196.